Carboxy-Terminus Recruitment Induced by Substrate Binding in Eukaryotic Fructose Bis-phosphate Aldolases[†,‡]

Julien Lafrance-Vanasse and Jurgen Sygusch*

Département de Biochimie, Université de Montréal, Montréal, Québec H3C 3J7, Canada

Received March 30, 2007; Revised Manuscript Received June 21, 2007

ABSTRACT: The crystal structures of *Leishmania mexicana* fructose-1,6-bis(phosphate) aldolase in complex with substrate and competitive inhibitor, mannitol-1,6-bis(phosphate), were solved to 2.2 Å resolution. Crystallographic analysis revealed a Schiff base intermediate trapped in the native structure complexed with substrate while the inhibitor was trapped in a conformation mimicking the carbinolamine intermediate. Binding modes corroborated previous structures reported for rabbit muscle aldolase. Amino acid substitution of Gly-312 to Ala, adjacent to the P_1-phosphate binding site and unique to trypanosomatids, did not perturb ligand binding in the active site. Ligand attachment ordered amino acid residues 359−367 of the C-terminal region (353−373) that was disordered beyond Asp-358 in the unbound structure, revealing a novel recruitment mechanism of this region by aldolases. C-Terminal peptide ordering is triggered by P_1-phosphate binding that induces conformational changes whereby C-terminal Leu-364 contacts P_1-phosphate binding residue Arg-313. C-Terminal region capture synergizes additional interactions with subunit surface residues, not perturbed by P_1-phosphate binding, and stabilizes C-terminal attachment. Amino acid residues that participate in the capturing interaction are conserved among class I aldolases, indicating a general recruitment mechanism whereby C-terminal capture facilitates active site interactions in subsequent catalytic steps. Recruitment accelerates the enzymatic reaction by using binding energy to reduce configurational entropy during catalysis thereby localizing the conserved C-terminus tyrosine, which mediates proton transfer, proximal to the active site enamine.

Aldolase is an essential enzyme that directs both glycolysis and gluconeogenesis, by reversibly catalyzing the conversion of fructose-1,6-bisphosphate (FBP[1]) into glyceraldehyde-3-phosphate (G3P) and dihydroxyacetone phosphate (DHAP) (*1*). A feature common to class I aldolases found primarily in vertebrates, insects, and higher plants is the use of a covalent mechanism for catalysis implicating Schiff base formation between a lysine residue on the enzyme and a ketose substrate (*2*). In glycolysis, the enzyme cleaves the FBP C_3-C_4 bond of the covalent intermediate liberating G3P and leaving an enamine carbanion bound in the active site. Stereospecific protonation of the chemically reactive enamine (*3*) regenerates a ketimine intermediate which upon hydrolysis liberates DHAP. Folding of the polypeptide chain of each aldolase subunit of the aldolase tetramer has been determined by crystallographic studies for mammalian aldolases (*4*−*7*), parasite aldolases (*8*, *9*), and *Drosophila* aldolase (*10*) and corresponds to a repetitive 8-fold $\beta\alpha$ motif commonly referred to as a β-barrel.

In class I aldolases, the active site is located in the center of the β-barrel at the bottom of a cleft and is accessible only from the carboxyl end of the β strands comprising the β-barrel. The active site is highly conserved among eukaryotic class I aldolases sequenced to date (*11*) and contains a number of charged residues, vicinal to the Schiff base forming lysine, that participate in catalysis (*12*, *13*). Binding by substrate and analogues in rabbit muscle aldolase induces a conformational change in two helical regions flanking the active site that narrows the active site cleft enabling Arg-303 to interact with the P_1-phosphate moiety and Ser-35 and Ser-38 with the P_6-phosphate (*12*).

A distinguishing structural feature of the enzyme is the C-terminal region (residues 343−363, rabbit muscle aldolase numbering), specific to subunits of mammalian aldolases and their orthologues, that is relatively flexible as indicated by high temperature factors and possesses an extended secondary structure (*10*, *12*, *14*). This region exhibits limited sequence homology and is considered conformationally mobile at the structural level as it contains stretches rich in glycine and alanine amino acids. The C-terminal region adopts various conformations in an aldolase structure, folding as an extended polypeptide chain over its proper subunit surface toward the active site more than 43 Å distant (*10*, *12*), folding toward a cleftlike region formed by subunit

[†] Research was supported by funding from Natural Science and Engineering Research Council (Canada) and Canadian Institutes for Health Research. Work was carried out in part at beam line X29 of the National Synchrotron Light Source, Brookhaven National Laboratory, which is supported by the U.S. Department of Energy, Division of Materials Sciences and Division of Chemical Sciences under Contract No. DE-AC02-98CH10886. J.L.-V. was the recipient of a Natural Science and Engineering Research Council (Canada) scholarship.

[‡] The Protein Data Bank entries for native, Schiff base intermediate, and MBP bound *Leishmania mexicana* aldolase are 2QAP, 2QDG, and 2QDH, respectively.

* To whom correspondence should be addressed. Phone: (514) 343-2389. Fax: (514) 343-2210. E-mail: jurgen.sygusch@umontreal.ca.

[1] Abbreviations: FBP, fructose-1,6-bis(phosphate); MBP, (2*R*)-mannitol-1,6-bis(phosphate); G3P, glyceraldehyde 3-phosphate; DHAP, dihydroxyacetone phosphate; HBP, hexitol-1,6-bis(phosphate); GBP, (2*S*)-glucitol-1,6-bis(phosphate); rms, root mean square

10.1021/bi700615r CCC: $37.00
Published on Web 07/28/2007

interfaces some 34 Å distant (*14*) as well as extending toward subunits of adjacent tetramers in the crystal lattice also more than 35 Å distant (*14*). The extensive conformational variability of the C-terminal polypeptide generated by crystal packing interactions underscores a relatively weak affinity of the C-terminal polypeptide for its proper subunit surface.

The C-terminal region has a significant role in catalysis as solution kinetic studies on muscle aldolase have shown that loss of the conserved C-terminus Tyr-363 specifically inhibits stereospecific proton exchange at the level of the enamine intermediate and making it rate limiting (*15*, *16*). Residues distal to this residue also have a functionally important role determining catalytic activity differences noted among aldolase isozymes (*17*, *18*). The kinetic data favor the hypothesis that proton exchange by Tyr-363 in the enamine intermediate necessitates interaction by the C-terminal region with the active site locus. However, the recruitment mechanism enabling Tyr-363 to interact with the active site locus remains to be established.

To investigate the structural role of the C-terminal region during catalysis, we have chosen to analyze ligand binding in the class I aldolase from *Leishmania mexicana*. The crystal structure of native *L. mexicana* aldolase has been determined (*8*) and in two subunits, both the active site loci and C-terminal residues 353−357 (344−349 in muscle aldolase), which are visible in the electron density map, are free of crystal packing contacts. For rabbit muscle aldolase, the crystal structures of native and substrate bound structures have been solved (*12*); however, crystal contacts precluded assignment of a structural role for the C-terminal region in catalysis. Residues 344−350 of the C-terminal region in both native and bound crystal structures of the muscle enzyme engage either directly or through intervening water molecules with a helical region (residues 40−50) in an adjacent tetramer subunit in the crystal lattice. The orientation of the helical region guides the trajectory of the C-terminal region toward the active site locus in one subunit. The same helix undergoes a displacement upon substrate binding (*12*) that rearranges its interaction with the C-terminal region and is concomitant with a shift in the C-terminal trajectory thereby contacting the P_1-phosphate binding site. By indirectly linking active site binding events and C-terminal attachment, crystal lattice interactions obviated casual analysis of the conformational changes induced by substrate binding.

A secondary goal was to examine the role of the amino acid substitution, Gly-302 → Ala, in the aldolase active site that is unique to *Leishmania* and *Trypanosome* species (*19*). Leishmaniasis is considered an emerging and uncontrolled disease with more than 12 million cases worldwide, mainly in underdeveloped countries; every year, more than 59,000 people die from it (*20*). *Leishmania* is an intracellular human pathogen found in erythrocytes and is transmitted into the bloodstream of human host by the bite of the sandfly, *Phlebotomus* (*21*). In its amastigote stage, the parasite relies principally on ATP production from glycolysis (*22*) making glycolytic enzymes a potential therapeutic target to fight *Leishmania* infections (*23*). Among these enzymes, aldolase is a target of choice, because of its central position in glycolysis following ATP investment, and because its products are used in other important metabolic pathways. In rabbit muscle aldolase, Gly-302 is adjacent to the P_1-phosphate binding site and its backbone atoms participate in P_1-phosphate binding (*12*) and mutation of this residue to a bulkier alanine in *Leishmania* and *Trypanosome* species (position 312, *Leishmania* aldolase numbering) may perturb P_1-phosphate binding. Knowledge of the mode of attachment at the P_1-phosphate locus would be useful in structure based design of specific aldolase inhibitor compounds that could lead to effective drugs.

Crystals of *L. mexicana* aldolase were incubated in the presence of substrate, FBP, and a tight binding competitive inhibitor, hexitol 1,6-bisphosphate (HBP) (*24*) to examine the structural role of active site binding on the C-terminal region. Flash freezing of *L. mexicana* aldolase crystals soaked briefly in saturating FBP solution trapped authentic Schiff base intermediate while in the presence of HBP, one of two HBP diastereoisomers, (2*R*)-mannitol-1,6-bis(phosphate) (MBP), was uniquely trapped in the aldolase active site. In both instances, binding resulted in active site recruitment of the C-terminal region free of crystal contacts and implicating conserved amino acid residues that provided insight into determinants of the reaction mechanism describing aldolase catalysis.

MATERIALS AND METHODS

HBP was prepared by $NaBH_4$ reduction of FBP as described previously (*24*). This reaction produces a mixture of two diastereoisomers: (2*R*)-mannitol-1,6-bisphosphate (MBP) and (2*S*)-glucitol-1,6-bisphosphate (GBP) (*24*). All figures in the present paper were prepared using the program PyMOL (*25*) and APBS (*26*).

Purification and Crystallization. Expression, purification, and crystallization of *L. mexicana* aldolase were carried out based on a method previously described (*8*). The PET15b plasmid containing the *L. mexicana* ALD gene, fused to a sequence coding for an N-terminal hexahistidine tag, was transformed and overexpressed in *Escherichia coli* BL21 pLysS. Nickel chelating affinity and size exclusion chromatography yielded a highly purified protein. Aldolase concentration was determined by BCA protein assay reagent with bovine serum albumin serving as a standard.

L. mexicana aldolase crystals were grown by vapor diffusion at 23 °C using a 1:4 mixture of protein solution (11 mg/mL initial protein concentration in 20 mM HEPES, pH 7.0) and precipitant buffer (15% polyethylene glycol 5000 MME in 20 mM sodium phosphate pH 4.0) respectively that was equilibrated against a reservoir of precipitant. Microseeding of previously grown crystals was used to improve crystal size and quality. pH measured in equilibrated drops was 4.5.

Data Collection and Processing. L. mexicana aldolase crystals were soaked for 2 min in FBP buffer (mother liquor plus 10 mM FBP) or for 5 min in HBP buffer (mother liquor plus 4.5 mM HBP). Prior to data collection, crystals were cryoprotected by transfer through a cryobuffer solution (FBP or HBP buffer plus 20% glycerol) and immediately flash frozen in a stream of gaseous N_2 cooled to 100 K. Diffraction data were collected from single crystals at beam line X29 of the National Synchrotron Light Source (Brookhaven National Laboratory, Upton, NY) using an ADSC Quantum-315 charge-coupled device (Area Detector Systems, Poway, CA). All data sets were processed with HKL2000 (*27*), and the results are summarized in Table 1.

Table 1: Data Collection and Refinement Statistics

	native	FBP	MBP
data collection			
resolution (Å)	50−1.71 (1.79−1.71)[a]	50−2.2 (2.31−2.2)[a]	50−2.14 (2.25−2.14)[a]
wavelength (Å)	1.1	1.1	1.1
reflections			
observed	3509740	2824392	3841275
unique	154162	69046	87658
completeness (%)	98.4 (81.7)	90.9 (71.6)	97.7 (77.2)
average $I/\sigma(I)$	28.6 (2.26)	18.2 (2.68)	12.6 (2.5)
R_{sym}[b]	0.080 (0.525)	0.081 (0.392)	0.080 (0.425)
redundancy	6.1 (3.4)	6.1 (4.4)	5.9 (3.9)
space group	$P2_12_12_1$	$P2_12_12_1$	$P2_12_12_1$
unit cell parameters			
a (Å), b (Å), c (Å)	85.8, 117.3, 160.2	85.1, 117.1, 161.8	85.1, 116.0, 161.7
refinement			
number of atoms			
protein	11075	11188	11188
water	2032	1714	1730
hetero	54	116	80
σ cutoff; $I/\sigma(I)$ >	1	1	1
R_{cryst} (%)[c]	0.173	0.185	0.190
R_{free} (%)[d]	0.203	0.238	0.235
rms deviation			
bond length (Å)	0.005	0.006	0.006
bond angle (deg)	1.376	1.367	1.253
⟨B⟩ (Å^2)	25.1	42.2	35.4
Ramachandran analysis[e] (%)			
most favorable	93.4	91.2	92.5
allowed	6.6	8.8	7.5
generously allowed	0	0	0
Luzzati plot (Å)	0.18	0.26	0.24
intersubunit variability (Å)	0.18	0.18	0.16

[a] All values in parentheses are given for the highest resolution shell [b] $R_{sym} = \sum_{hkl}\sum_i|I_i(hkl) - \bar{I}_i(hkl)|/\sum_{hkl}\sum_i I_i(hkl)$ with i running over number of independent observations of reflection hkl. [c] $R_{cryst} = \sum_{hkl}||F_o(hkl)| - |F_c(hkl)||/\sum_{hkl}|F_o(hkl)|$. [d] $R_{free} = \sum_{hkl\in T}||F_o(hkl)| - |F_c(hkl)||/\sum_{hkl\in T}|F_o(hkl)|$, where T is a test data set randomly selected from the observed reflections prior to refinement. Test data set was not used throughout refinement and contained 5%, the total unique reflections. [e] Analyzed by PROCHECK.

Structure Solution and Refinement. Initial phases used for model building of native and liganded structures were obtained by molecular replacement using the previously determined structure for the *L. mexicana* aldolase tetramer (PDB 1EPX). The crystal structures belong to the orthorhombic space group $P2_12_12_1$ and have one aldolase homotetramer in the asymmetric unit. All reflections having $I/\sigma(I) > 1$ were used in refinement; however, electron density maps were calculated to the resolution shown in Table 1 and corresponded to completeness of at least 70% in the highest resolution shell. The structures were subjected to iterative rounds of refinement (simulated annealing and minimization) with CNS (*28*) and model building using O (*29*). Water molecules were automatically added by CNS in initial rounds and manually near the end of refinement. C-Terminal regions (residues 358−366) were traced in subunits A and B only, for the FBP and HBP soaked crystal structures.

Ligand modeling was based on interpretation of electron density shapes of $2F_o - F_c$ and $F_o - F_c$ annealed omit maps, and the program PRODRG was used for topology and parameter generation (*30*). Binding by FBP and HBP, as the MBP diastereoisomer, was readily discernible and was associated with clearly defined electron densities in the active site. Difference electron density ($F_o - F_c$) annealed omit maps calculated in the final round of refinement confirmed identical binding of ligands in all four subunits.

Final model statistics, calculated with CNS and PROCHECK (*31*), are shown in Table 1. The coordinates and structure factors of native aldolase, covalently bound FBP, and MBP as noncovalent complex have been deposited with the Protein Data Bank (PDB 2QAP, PDB 2QDG, and PDB 2QDH, respectively). Final models for the structure of native aldolase and complexes formed with FBP bound covalently and MBP noncovalent have an R_{cryst} (R_{free}) of 0.173 (0.203), 0.185 (0.238), and 0.190 (0.235), respectively. The corresponding Luzzati atomic coordinate error was estimated at 0.18, 0.26, and 0.24 Å, respectively. Ramachandran analysis performed with PROCHECK placed at least 90% of non-glycine and non-proline residues of the three structures in the most favorable region and with the remainder found in the allowed region while no residues were in the generously allowed region, attesting to good model geometry in the structures. Errors in hydrogen bond distances, positional differences, and *B*-factors are reported as SD values and were estimated based on their value found in each aldolase subunit.

Structure Comparisons. Superpositions were performed with the program PyMOL (*25*) using C_α atom coordinates of identical blocks of amino acid sequences and comparing native with liganded aldolase tetramers. Due to conformational heterogeneity among subunits in N-terminal and C-terminal regions, comparisons were performed using residues 24−353 in *L. mexicana* aldolase and residues 14−343 in rabbit muscle aldolase.

A difference distance matrix of C_α coordinates from native and liganded structures was calculated using the program

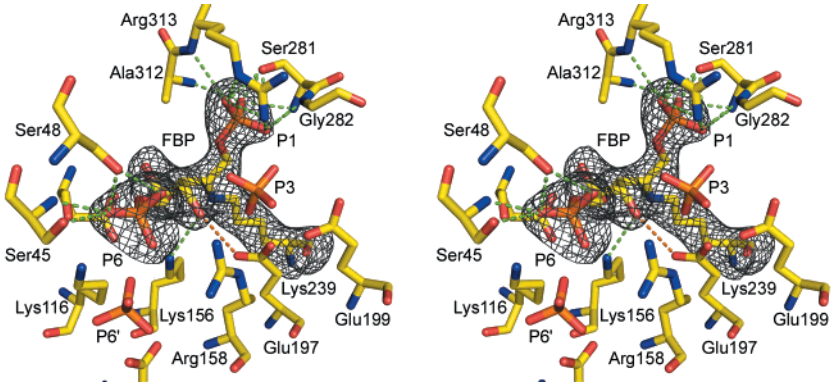

FIGURE 1: Electron density showing the Schiff base intermediate trapped in the active site of *L. mexicana* aldolase. Shown in stereo is the difference electron density was calculated from a 2.2 Å annealed $F_o - F_c$ omit map encompassing Lys-239 and FBP and contoured at 3.5σ. The continuous electron density is consistent with trapping of a Schiff base that is covalently bound to Lys-239 in all subunits. The green dashes illustrate hydrogen bonds, and the orange dash indicates close contact between Glu-197 and hydroxyl of C_4. The orientation corresponds to viewing roughly parallel to the subunit β-barrel axis and looking down into the β-barrel from the carboxyl ends of the β-strands.

DDMP (*32*) to find invariant structural elements. Residues 112−269, representing β-strands and α-helices 3, 4, 5, and 6 of the β-barrel structure, showed least variation (rms = 0.18 Å based on C_α atoms) among all structures and were used in all subsequent structure superpositions to discover regions in the liganded structures that underwent conformational changes upon ligand binding. The same protocol was applied for comparisons between parasite aldolase and rabbit muscle aldolases and revealed that residues 112−240 in *L. mexicana* aldolase, and the corresponding stretch of residues 102−230 in the rabbit muscle structures, represented the polypeptide sequence stretches having least variations (rms = 1.0 Å based on C_α atoms for the two structures). Intersubunit variability within a tetramer based on these sequence stretches was analyzed by the program Polypose (*33*) and yielded rms differences for each tetramer, based on C_α atom coordinates, that were less than the error in the atomic coordinates for each structure.

Surface Calculation. Surface calculations were performed with the program CNS. The buried surface was calculated between residues 1−354 and residues 355−366 of the C-terminal region for the liganded structures. The calculation was repeated with Leu-364 residue mutated to glycine. The difference of the two values gave the solvent accessible surface buried by the interaction between Arg-313 and Leu-364.

RESULTS AND DISCUSSION

Native Enzyme. The combination of refined crystallization conditions and high flux of the synchrotron beamline improved signal-to-noise ratios for diffracted intensities of native crystals of *L. mexicana* aldolase, shown in Table 1, compared to the original structure (*8*). The improved resolution allowed placement of several side chains missing in the original structure as well as the addition of an extra residue, Asp-358, in the C-terminal polypeptide. Different from the original structure, electron density was found at three distinct sites in each subunit and was interpreted as bound phosphate oxyanions consistent with 20 mM sodium phosphate used to buffer the crystallization solution. Two phosphates, at sites P_2 and P_3, are bound in the active site at positions distinct from the P_1- and P_6-phosphate binding sites used in substrate and analogue binding (*12*). Although the P_2-phosphate binding site overlaps with P_1-phosphate site and oxyanions in both sites interact with the same residues Ser-281 and Gly-282, Arg-313 (Arg-303 in rabbit muscle aldolase), which grasps the P_1-phosphate, does not interact with the P_2-phosphate. Rather the guanidinium moiety of Arg-313 remains disordered in the electron density and points toward the solvent as observed in the crystal structure of the native rabbit muscle aldolase (PDB 1ZAH). The P_3-phosphate hydrogen bonds with the P_2-phosphate as well as with conserved residues Glu-197 and Glu-199. A hydrogen-bonding pattern implicating the P_3-phosphate and glutamate residues requires that at least one glutamate residue must be protonated and that at least one of the phosphate oxyanions is monobasic at pH 4.5 consistent with the acidic crystallization conditions.

Schiff Base. Continuous electron density, extending beyond Lys-239 N_z in each subunit, shown in Figure 1, indicated formation of a stable covalent adduct with FBP consistent with trapping of a Schiff base intermediate in each aldolase subunit. Arg-313 side chain curls to grasp the P_1 oxyanion and which is further stabilized by hydrogen bonding with backbone amides of residues Ser-281, Gly-282, Ala-312, and Arg-313 and side chain of Ser-281, identical to FBP binding in rabbit muscle aldolase (*12*). To make room for Arg-313 to interact with the P_1-phosphate, the backbone conformation of Gly-282 flips such that the Gly-282 carbonyl no longer contacts the Arg-313 guanidinium moiety and points in the opposite direction. The peptide flip by Gly-282 displaces the Gly-283 carbonyl oxygen by 1.4 Å toward the incoming C-terminal region and mimics conformational changes observed for the Schiff base structure formed with FBP in rabbit muscle aldolase (*12*).

The remaining interactions, shown in Figure 1, between active site residues and P_6-phosphate and FBP hydroxyls are also present in the FBP bound rabbit muscle aldolase structure. Superposition of FBP structures from rabbit muscle aldolase and *L. mexicana* aldolase (rms deviation = 1.15 Å for C_α atoms of residues 14−343 for rabbit muscle aldolase and 24−353 for *L. mexicana* aldolase and rms deviation = 0.76 Å for FBP atoms) reinforce identical binding modes by FBP in active sites of both aldolases. The active site cavity can readily accommodate the amino acid substitution Gly-312 → Ala as it does not perturb the mode of substrate binding or interactions. Additional electron density found in the active site was interpreted as binding by two phosphate

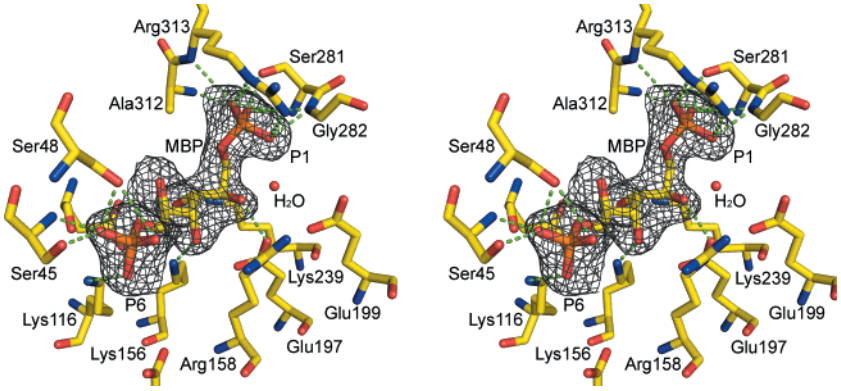

FIGURE 2: Electron density showing MBP bound in the active site of *L. mexicana* aldolase. Shown in stereo is the difference electron density was calculated from a 2.2 Å annealed $F_o - F_c$ omit map encompassing MBP and contoured at 2.5σ. The ligand is present in all subunits. The MBP mode of attachment is stabilized similarly as observed for the Schiff base intermediate. Green dashes illustrate hydrogen bonds. The orientation is the same as in Figure 1.

moieties, one at the previous P_3 binding site and a new P_6' site, shown in Figure 1. P_6'-phosphate promotes a slight conformational displacement of Arg-158 to interact with the oxyanion. P_6'-phosphate interaction with the P_6-phosphate requires one of the oxyanions to be monobasic and suggests that all phosphate anion binding sites are a likely consequence of the acidic crystallization condition.

Carbinolamine Analogue. The electron density shown in Figure 2 indicates formation of a stable noncovalent hexose−P_2 adduct in the active site. The nonplanar shape of the electron density about the C_2 atom of the hexose−P_2 indicates tetrahedral hybridization and is consistent with trapping of (2*R*)-MBP in each aldolase subunit. Superposition of FBP and MBP structures (rms deviation = 0.28 Å for C_α atoms of residues 24−353) reflects similar interactions made by the ligands with active site residues including the conformational change imposed on Gly-283 due to P_1-phosphate binding. The C_2 hydroxyl present in MBP but not in the Schiff base with FBP makes an additional hydrogen bond with Glu-197 also observed in rabbit muscle aldolase (*12*). Furthermore, superposition of *L. mexicana* aldolase (residues 24−353) with rabbit muscle aldolase (residues 14−343) bound by MBP (rms deviation = 1.11 Å comparing C_α atoms and 0.54 Å for MBP atoms only) is consistent with identical binding modes for the MBP ligand including the same short hydrogen bond made by Ser-281 (Ser-271 in rabbit muscle aldolase) with the P_1-phosphate oxyanion (2.47 ± 0.23 Å with FBP, 2.46 ± 0.25 Å with MBP). The bound configuration of (2*R*)-MBP mimics the transient carbinolamine precursor in FBP aldolase and thus acts as a transition state analogue maximizing its active site interactions. Similar to the FBP structure, the presence of the methyl group in Ala-312 does not affect binding integrity of the inhibitor and makes this amino acid substitution neutral with regard to substrate or analogue attachment.

Induced Fit. To assess conformational changes concomitant with FBP and MBP binding, a difference matrix of C_α coordinates was calculated using native, FBP, and MBP bound structures. The interaction of Arg-313 with the P_1-phosphate induces a global conformational displacement shifting surrounding α-helical residues 310−330 by 0.69 ± 0.21 Å toward the active site. An adjacent region, also of α-helical secondary structure and corresponding to residues 43−61, upon P_6-phosphate binding by residues Ser-45 and Ser-48, undergoes a global conformational change by 1.41 ± 0.05 Å that narrows the active site cleft in subunits A and B and to a lesser extent, by 0.57 ± 0.28 Å, in subunits C and D. In the crystal structure, subunits C and D from different tetramers make reciprocal crystal packing contacts that involve residues of this region (*43*−*61*) and would penalize structural movement breaking these contacts. The similar conformational change in all subunits is consistent with an induced fit mechanism activated by attachment of the substrate or analogue phosphate oxyanions that was also observed for homologous helical regions in the crystal structure of rabbit muscle aldolase (*12*). The absence of significant conformational changes by all other active site residues corroborates the interpretation of a rigid active site that does not adapt to binding events except by large scale movement of secondary structures.

C-Terminal Region. Active site binding resulted in additional continuous electron density visible beyond Asp-358 of the C-terminal region in two subunits, A and B, and was interpreted as the polypeptide sequence corresponding to C-terminal residues 359−366, shown in Figure 3. Remaining C-terminal residues 367−373 could not be convincingly fitted into electron density map and were considered disordered. The majority of interactions by the additional C-terminal region involve main chain interactions with residues on the subunit surface that stabilize P_1-phosphate binding, which is shown in Figure 4.

Residues directly and indirectly involved in stabilizing P_1-phosphate binding capture a specific segment of the C-terminal region. P_1-phosphate binding enables the Arg-313 side chain to grasp the oxyanion that induces a flip of the Gly-282 peptide allowing oxyanion interaction with the Gly-282 amide. The peptide flip displaces the carbonyl oxygen of adjacent Gly-283 from its position in the native enzyme such that Gly-283 hydrogen bonds with the Leu-364 backbone amide. C-Terminal capture is prefaced by hydrogen bonding of the Ser-363 side chain with backbone amide of Tyr-365 to form a cyclic structure that includes Leu-364 and Tyr-365 backbone atoms. The cyclic structure aligns the backbone amide of Leu-364 for hydrogen bonding with the Gly-283 carbonyl oxygen and further orients the Leu-364 side chain for interaction with the aliphatic carbons of the Arg-313 side chain. The hydrophobic interaction buries an additional 125 $Å^2$ of solvent accessible surface representing 2.5−4.3 kcal/mol of solvation energy (*34*). The gain in solvation energy is however an overestimate as Arg-313 and

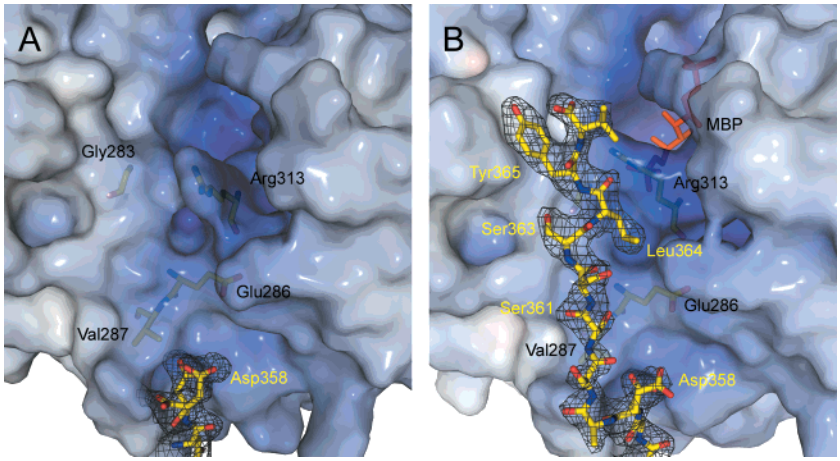

FIGURE 3: C-Terminal residues 359−366 of *L. mexicana* aldolase become ordered upon ligand binding. Electron density map corresponding to the ordered C-terminal region combined with a solvent accessible electrostatic surface potential representation of an aldolase subunit calculated using residues 1−353. Panel A was derived from the structure of the native enzyme while panel B was obtained using the structure of the enzymatic complex formed with MBP. MBP is bound in the active site cleft and is illustrated in red. Difference electron density was calculated from a 2.2 Å annealed $F_o - F_c$ omit map contoured at 3.5σ encompassing the C-terminal residues 357−358 from native structure and residues 357−366 from the MBP structure. Residues 359−366 of the C-terminal region are visible in subunits A and B, while in subunits C and D, the electron density becomes disordered beyond residue 358, as was observed in the native structure. Similar electron density maps were obtained in the structure with the Schiff base intermediate. The subunit surface potentials were calculated using APBS (*26*) and the scale ranges −10 to 10 on the solvent accessible surface. Blue represents positively charge surface while white is a neutral surface (red is negative, absent in this figure). The C-terminal residues are labeled in yellow, and the interacting residues on the subunit surface are labeled in black. The orientation is approximately perpendicular to the axis of the subunit β-barrel, slightly tilted toward the active site, whose periphery is located in the upper hand of the figure near Arg-313.

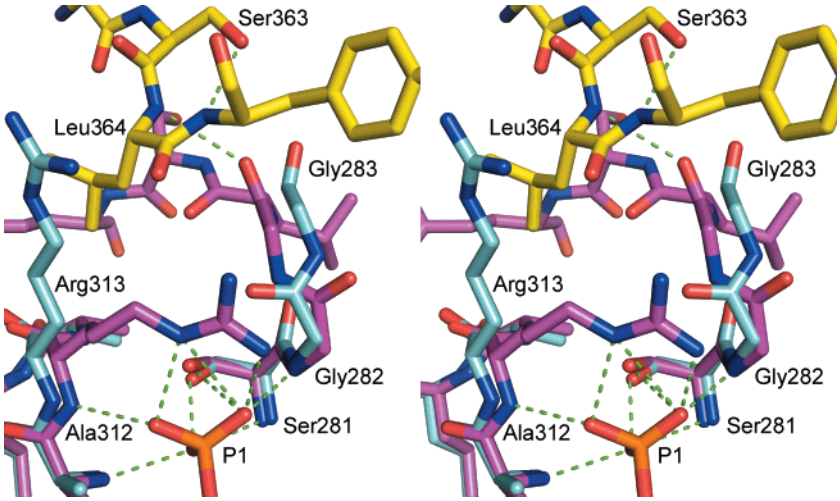

FIGURE 4: P_1-phosphate binding is responsible for recruitment of the C-terminal region to the active site. Shown in stereo is the region binding the P_1-phosphate at the active site periphery of native aldolase (cyan) and MBP (magenta) bound structures. The C-terminus recruited in the MBP bound structure is shown in yellow and is identical to the binding mode observed in the Schiff base intermediate formed with FBP. The green dashes illustrate hydrogen bonds. The orientation of the figure is perpendicular to the axis of the subunit β-barrel.

Leu-364 are disordered in the native structure. A similar mode of active site interaction by the C-terminal region was observed in the crystal structures of rabbit muscle aldolase bound by FBP and MPB (*12*).

Additional C-terminal interactions with the subunit surface residues are few and include Ser-361 side chain hydrogen bonding backbone amides of Glu-286 and Val-287 and Tyr-365 phenyl side chain stacking against Ala-247 while its hydroxyl interacts with Asp-248. The hydrogen bonding interactions made by the C-terminal region are pH independent, and hence the substrate induced C-terminal ordering is not an artifact of the acidic crystallization conditions. The gain in binding free energy consequent with C-terminal recruitment is however offset against the disorder of the C-terminal residues and Arg-313 in the native enzyme and corroborates the notion of low affinity binding by the C-terminal region with the active site locus.

Trajectories of C-terminal regions of subunits A and B of *L. mexicana* aldolase are more than 10 Å from adjacent tetramers minimizing potential bias with regard to stabilization of the C-terminal region conformation by crystal contacts. In the remaining two subunits, C and D, adjacent tetramers block attachment of C-terminal residues beyond residue Asp-358 even though all subunits were bound by ligands. Full occupancy of the P_1-phosphate binding site by both ligands in subunits C and D indicates that the C-terminal region is not required for active site binding.

C-Terminal Recruitment. The interaction network composed of amino acids Gly-282, Gly-283, Arg-313, Ser-363, and Leu-364 and produced by capture of the C-terminal region is conserved in all class I aldolases sequenced to date (*11*). Although other C-terminal residues engage in binding with the subunit surface upon ligand attachment, these are not conserved and are structurally insensitive to P_1-phosphate binding events. Their interaction suggests a cooperative recruitment mechanism necessitating P_1-phosphate binding to capture the C-terminal region through conserved interactions and which is further stabilized by additional nonconserved interactions. The conservation of the amino acid residues engaged in C-terminal capture points to a mechanistic feature general to class I aldolase catalysis.

By anchoring the C-terminal region at the active site periphery, the gain in binding energy reduces configurational entropy and acts as a hinge for more precise delivery, following substrate cleavage, of the remaining C-terminal heptapeptide into the active site to mediate proton exchange. Substrate immobilization in an active site reduces configurational entropy by increasing the effective concentration of substrate competent for catalysis and can accelerate a reaction by many orders of magnitude (*35*). In this context, C-terminal recruitment by substrate, prior to catalysis, would lessen the consequent entropy loss in active site docking by the C-terminus tyrosine and lower the activation barrier for proton exchange at the enamine. The reduction in proton exchange by mutation of the conserved C-terminal Leu to Ala in maize aldolase (*18*) corroborates the interpretation that loss of the Arg−Leu hydrophobic interaction diminishes recruitment of the C-terminal region thereby enhancing configurational entropy in the substrate bound state which would raise the height of transition state barrier associated with the proton transfer step and thus lower catalytic activity.

Increasing the effective concentration of the conserved terminal tyrosine residue in the active site, by C-terminal capture at the active site locus, would afford greater protection against proteolysis and is consistent with increased resistance to carboxypeptidase A degradation of the C-terminus in all aldolases in the presence of dihydroxyacetone-P (*15*). Although the sequence of the C-terminal region (residues 367−372) is variable among species, the number of residues between the Ser-Leu dyad and terminal tyrosine is constant (6 residues) in all class I aldolases. The most parsimonious interpretation is that participation by the C-terminal tyrosine in proton exchange requires sufficient residues to reach the enamine from the Ser-Leu dyad, a consideration resulting from the underlying conserved reaction geometries in class I aldolases, that of a fixed distance between the P_1-phosphate and the exchangeable 3(S) hydrogen of the C_3 carbon in the enamine. Active site interactions by conserved residues and backbone atoms of the penultimate C-terminal region, such as with backbone atoms of residues 364−365, would be consistent with a constant number of nonhomologous intervening residues and which would not be subject to significant evolutionary pressure regarding sequence consensus. Substrate mediated attachment by the C-terminal region ensures that C-terminal region is not recruited to the active site in the native enzyme thereby minimizing steric interference with substrate binding. Furthermore, the apparent low affinity by the C-terminal region for interaction with its proper subunit surface in the native enzyme corroborates that entropy loss diminishes binding affinity (*36*) and supports loss of configurational entropy as a significant factor in entropy reduction upon active site binding (*37*).

In conclusion, a novel recruitment mechanism is described involving interaction of the C-terminal region with the active site locus in class I aldolases. Substrate binding induces partial ordering of the C-terminal peptide at the active site periphery. The reduction in configurational entropy by ordering of the C-terminal region precedes catalytic events and thus reduces configurational entropy loss during the catalytic cycle. Minimizing entropy loss diminishes the activation barrier of the proton transfer rate step that is mediated by the C-terminal tyrosine and accelerates the enzymatic reaction. This entropy reduction mechanism is conserved among class I aldolases as the amino acid residues participating in C-terminal capture are also conserved.

ACKNOWLEDGMENT

We wish to thank Dr. Paul Michels and Nathalie Chevalier at the Research Unit for Tropical Diseases, University of Louvain, for furnishing the expression plasmid PET15b containing the *L. mexicana* aldolase gene. We also thank Miguel St-Jean for critical reading of the manuscript.

REFERENCES

1. Meyerhof, O., Lohmann, K., and Sehuster, P. H. (1936) Uber die Aldolase, *Biochem. Z. 236*, 301−319.
2. Grazi, E., Rowley, P. T., Chang, T., Tchola, O., and Horecker, B. L. (1962) The mechanism of action of aldolases. III. Schiff base formation with lysine, *Biochem. Biophys. Res. Commun. 9*, 38−43.
3. Rose, I. A., and Rieder, S. V. (1958) The mechanism of action of aldolase and the asymmetric labeling of hexose, *J. Biol. Chem. 231*, 315−329.
4. Sygusch, J., Beaudry, D., and Allaire, M. (1987) Molecular architecture of rabbit skeletal muscle aldolase at 2.7-A resolution, *Proc. Natl. Acad. Sci. U.S.A. 84*, 7846−7850.
5. Gamblin, S. J., Cooper, B., Millar, J. R., Davies, G. J., Littlechild, J. A., and Watson, H. C. (1990) The crystal structure of human muscle aldolase at 3.0 Å resolution, *FEBS Lett. 262*, 282−286.
6. Dalby, A. R., Tolan, D. R., and Littlechild, J. A. (2001) The structure of human liver fructose-1,6-bisphosphate aldolase, *Acta Crystallogr., Sect. D: Biol. Crystallogr. 57*, 1526−1533.
7. Arakaki, T. L., Pezza, J. A., Cronin, M. A., Hopkins, C. E., Zimmer, D. B., Tolan, D. R., and Allen, K. N. (2004) Structure of human brain fructose 1,6-(bis)phosphate aldolase: linking isozyme structure with function, *Protein Sci. 13*, 3077−3084.
8. Chudzik, D. M., Michels, P. A., de Walque, S., and Hol, W. G. (2000) Structures of type 2 peroxisomal targeting signals in two trypanosomatid aldolases, *J. Mol. Biol. 300*, 697−707.
9. Kim, H., Certa, U., Dobeli, H., Jakob, P., and Hol, W. G. (1998) Crystal structure of fructose-1,6-bisphosphate aldolase from the human malaria parasite Plasmodium falciparum, *Biochemistry 37*, 4388−4396.
10. Hester, G., Brenner-Holzach, O., Rossi, F. A., Struck-Donatz, M., Winterhalter, K. H., Smit, J. D., and Piontek, K. (1991) The crystal structure of fructose-1,6-bisphosphate aldolase from Drosophila melanogaster, at 2.5 Å resolution, *FEBS Lett. 292*, 237−242.
11. Hannaert, V., Bringaud, F., Opperdoes, F. R., and Michels, P. A. (2003) Evolution of energy metabolism and its compartmentation in Kinetoplastida, *Kinetoplastid Biol. Dis. 2*, 11−41.
12. St-Jean, M., Lafrance-Vanasse, J., Liotard, B., and Sygusch, J. (2005) High resolution reaction intermediates of rabbit muscle fructose-1,6-bisphosphate aldolase: substrate cleavage and induced fit, *J. Biol. Chem. 280*, 27262−27270.
13. Maurady, A., Zdanov, A., de Moissac, D., Beaudry, D., and Sygusch, J. (2002) A conserved glutamate residue exhibits multifunctional catalytic roles in D-fructose-1,6-bisphosphate aldolases, *J. Biol. Chem. 277*, 9474−9483.

14. Blom, N., and Sygusch, J. (1997) Product binding and role of the C-terminal region in class I D-fructose 1,6-bisphosphate aldolase, *Nat. Struct. Biol. 4*, 36−39.
15. Drechsler, E. R., Boyer, P. D., and Kowalsky, A. G. (1959) The catalytic activity of carboxypeptidase-degraded aldolase, *J. Biol. Chem. 234*, 2627−2634.
16. Rose, I. A., O'Connell, E. L., and Mehler, A. H. (1965) Mechanism of the aldolase reaction, *J. Biol. Chem. 240*, 1758−1765.
17. Berthiaume, L., Tolan, D. R., and Sygusch, J. (1993) Differential usage of the carboxyl-terminal region among aldolase isozymes, *J. Biol. Chem. 268*, 10826−10835.
18. Berthiaume, L., Loisel, T. P., and Sygusch, J. (1991) Carboxyl terminus region modulates catalytic activity of recombinant maize aldolase, *J. Biol. Chem. 266*, 17099−17105.
19. de Walque, S., Opperdoes, F. R., and Michels, P. A. (1999) Cloning and characterization of *Leishmania mexicana* fructose-1,6-bisphosphate aldolase, *Mol. Biochem. Parasitol. 103*, 279−283.
20. WHO. (2004) *World Health Report 2004: Changing history*, World Health Organization, Geneva.
21. Remme, J. H. F., Blas, E., Chitsulo, L., Desjeux, P. M. P., Engers, H. D., Kanyok, T. P., Kayondo, J. F., Kioy, D. W., Kumaraswami, V., Lazdins, J. K., Nunn, P. P., Oduola, A., Ridley, R. G., Toure, Y. T., Zicker, F., and Morel, C. M. (2002) Strategic emphases for tropical diseases research: a TDR perspective, *Trends Microbiol. 10*, 435−440.
22. Tielens, A. G., and Van Hellemond, J. J. (1998) Differences in energy metabolism between trypanosomatidae, *Parasitol. Today 14*, 265−272.
23. Verlinde, C. L., Hannaert, V., Blonski, C., Willson, M., Perie, J. J., Fothergill-Gilmore, L. A., Opperdoes, F. R., Gelb, M. H., Hol, W. G., and Michels, P. A. (2001) Glycolysis as a target for the design of new anti-trypanosome drugs, *Drug Resist. Updates 4*, 50−65.
24. Ginsburg, A., and Mehler, A. H. (1966) Specific anion binding to fructose diphosphate aldolase from rabbit muscle, *Biochemistry 5*, 2623−2634.
25. DeLano, W. L. (2002) The PyMOL Molecular Graphics System on World Wide Web, http://www.pymol.org.
26. Baker, N. A., Sept, D., Joseph, S., Holst, M. J., and McCammon, J. A. (2001) Electrostatics of nanosystems: application to microtubules and the ribosome, *Proc. Natl. Acad. Sci. U.S.A. 98*, 10037−10041.
27. Otwinowski, Z., and Minor, W. (1997) Processing of X-ray diffraction data collected in oscillation mode, *Methods Enzymol. 276*, 307−326.
28. Brunger, A. T., Adams, P. D., Clore, G. M., DeLano, W. L., Gros, P., Grosse Kunstleve, R. W., Jiang, J.-S., Kuszewski, J., Nilges, N., Pannu, N. S., Read, R. J., Rice, L. M., Simonson, T., and Warren, G. L. (1998) Crystallography & NMR system: A new software suite for macromolecular structure determination, *Acta Crystallogr., Sect. D: Biol. Crystallogr. 54*, 905−921.
29. Jones, T. A., Zou, J. Y., Cowan, S. W., and Kjeldgaard, M. (1991) Improved methods for building protein models in electron density maps and the location of errors in these models, *Acta Crystallogr., Sect. A 47*, 110−119.
30. Schuttelkopf, A. W., and van Aalten, D. M. (2004) PRODRG: a tool for high-throughput crystallography of protein-ligand complexes, *Acta Crystallogr., Sect. D: Biol. Crystallogr. 60*, 1355−1363.
31. Laskowski, R. A., MacArthur, M. W., Moss, D. S., and Thornton, J. M. (1993) SFCHECK: a unified set of procedures for evaluating the quality of macromolecular structure-factor data and their agreement with the atomic model, *J. Appl. Crystallogr. 26*, 283−291.
32. Richards, F. M., and Kundrot, C. E. (1988) Identification of structural motifs from protein coordinate data: secondary structure and first-level supersecondary structure, *Proteins 3*, 71−84.
33. Diamond, R. (1992) On the multiple simultaneous superposition of molecular structures by rigid body transformations, *Protein Sci. 1*, 1279−1287.
34. Sharp, K. A., Nicholls, A., Fine, R. F., and Honig, B. (1991) Reconciling the magnitude of the microscopic and macroscopic hydrophobic effects, *Science 252*, 106−109.
35. Page, M. I., and Jencks, W. P. (1971) Entropic contributions to rate accelerations in enzymic and intramolecular reactions and the chelate effect, *Proc. Natl. Acad. Sci. U.S.A. 68*, 1678−1683.
36. Jenks, W. P. (1997) From chemistry to biochemistry to catalysis to movement, *Annu. Rev. Biochem. 66*, 1−18.
37. Chang, C. A., Chen, W., and Gilson, M. K. (2007) Ligand configurational entropy and protein binding, *Proc. Natl. Acad. Sci. U.S.A. 104*, 1534−1539.

BI700615R